# Characterization of Ultrasonic Wave Propagation in the Application of Prevention of Fouling on a Ship's Hull

**Ignacio Garcia De Carellan [1], Serafeim Moustakidis[2], Mathew Legg[1], Raghav Dave[1], Vassilios Kappatos[1], Cem Selcuk[1], Pierre-Oliver Jost [3], Hans Juerg Krause[3], Jan Seton[4], Tat-Hean Gan[1] and Kostas Hrissagis[2]**

*1. Brunel University, Uxbridge, Middlesex, UB8 3PH, United Kingdom*
*2. Center for Research and Technology, Hellas (CERTH), Greece*
*3. Sofchem, 9, rue du Gué, 92500 Rueil Malmaison #, France*
*4. WRS Marine, Edisonwef 12, 3291CK Strijen, The Netherlands*

**Abstract:** Biofouling build-up, an undesirable formation of organisms on a surface immersed in water, has diverse negative effects on engineering structures, which in turn results in socio-economic impacts across industry sectors; such as offshore and maritime. Several approaches for antifouling have been explored to date; spanning across the use of electric fields, ultraviolet radiation, bespoke coatings and paints. These methods have their respective shortcomings, either in terms of applicability range, scale up, financial feasibility, environmental effects or sustainability. Especially after the ban on certain antifouling paints, industrial and scientific focus has shifted to alternative preferably non-invasive and innovative approaches including guided wave ultrasonic technology. In this conference paper the ultrasonic wave propagation through key features in a ship's hull is presented. Results from 3D laser scanning vibrometer measurements and modelling of ultrasonic wave propagation are presented. Additionally, this work has been focused on modelling the forces exerted by ultrasonic plate waves in a ship hull, on the organic macromolecules and microorganisms present in water, before they form a microfouling and which can lead to macrofouling.

**Keywords:** fouling prevention; ship hull; guided waves; ultrasonic
**Article ID:** HS-BL-B

## 1 Introduction

Biofouling build-up, an undesirable formation of organisms on a surface immersed in water, is a significant problem for all marine structures such as ships, offshore rigs and oceanographic sensors (Shifeng, Nov 2012). Biofouling has a huge economic cost for the shipping industry. As a consequence of fouling build up, considerably more fuel is consumed thereby resulting in both an economic and environmental impact. Ships have to be frequently taken out of service to be cleaned due to formation of fouling on them in the marine environment. The marine industry globally spends significant capital (equivalent to billions of euros) in addressing fouling, using a variety of methods for cleaning, prevention or protection e.g. coatings.

There are different types of conventional measures taken to combat biofouling, including antifouling coatings, chemical agents etc. However, environmental concerns associated with toxic antifouling coatings have led to studies into alternative methods for biofouling control, which include acoustic techniques (Yebra, 2004) (Gittens, 2013). The Cleanship project (www.cleanship-project.eu), is a pan-European collaboration across France, Holland, Spain, Greece and Turkey, coordinated by the Brunel Innovation Centre (BIC) based in Cambridge, England, UK proposes an effective non-invasive solution, based on an ultrasonic approach, for improving the maintenance of ships. The solution is to deploy high power ultrasonic waves travelling throughout steel plates of a ship hull for, as much as possible, (i) prevention of fouling and (ii) detection of fouling.

Acoustic techniques have been proposed as an alternative non-toxic method for biofouling control. The methods in practice may be categorized into two groups (i) audible / ultrasonic range wave emission systems (ii) acoustic sparkers (named pulsars, too). Studies on the use of these acoustic techniques have been very promising. Currently, there are commercial ultrasonic antifouling systems for yachts, such as that provided by Sofchem (Sofchem, distributeur et installateur de la technologie anti algues Fluid Impact). A number of patents relating to the use of acoustics for biofouling control can be found in (David Blythe Foster, 1954) (Morley, 1954) (Piper, 1977).

Several devices emitting mechanical waves in the audible and ultrasonic frequency range, have been used for biofouling control. Acoustic devices have been attached to substrates

**Received date:**
**Foundation item:** Supported by
***Corresponding author Email: bic@brunel.ac.uk**
**vassilis.kappatos@brunel.ac.uk**

such as yacht and ship hulls, panels, and pipes and have been used for ultrasonic bath lab tests, including audio speakers (Piper, 1977), piezoelectric transducers (Branscomb, 1984) (Choi, 2013) (Gavand, 2007) (Kitamura, 1995) and strips/films (Morley, 1954) (Piper, 1977) (Latour, 1981), and magnetostrictive transducers (P. S. Sheherbakov, 1974). Multiple transducers array may be used together to optimize overall gain. Positioning & spacing between the transducers need to be considered, due to the effects of constructive and destructive interference. Interference may produce areas, referred to as 2 anti-nodes, where the displacement will be a minimum, potentially reducing the biofouling growth at these areas. The antifouling effectiveness may be expected to decrease with increasing distance from the transducer locations (Delauney, 2009).

Antifouling works have been performed in the ultrasonic frequency range (Kitamura, 1995) (G Mazue, 2011) (Bott, 2000) (Latour, 1981) (P. S. Sheherbakov, 1974) (Fischer, 1984). Several sea trials have been reported where lower ultrasonic frequencies were used successfully for prevention of biofouling growth. Merchant ship hulls vibrated for periods of several years were reported to have reduced fouling levels (Band). Sheherbakov et. al. stated that about 20 vessels in the Soviet fleet had been equipped with ultrasonic antifouling protection systems (P. S. Sheherbakov, 1974). The hulls were vibrated using oscillators fixed to the inner hull operating. They observed that fouling prevention was evident, but that a stripped fouling pattern occurred due to reduced vibration amplitude at the bulkheads and framing.

The rest of the paper is organized as follows: in section 2 the biofouling formation mechanism and build up is described. Modelling investigation and results are given in Section 3, whereas Section 4 describes the experimental setup and associated results based on the proposed vibrometry analysis. A summary of conclusions is given in the last section 5.

## 2 Biofouling

In general, fouling can be defined as the accumulation of organic or inorganic matter on a surface. Biofouling is the creation of microorganisms, plants, and other marine life on a surface in contact with water (Yebra, 2004). Upon immersion of a surface into water, a film composed mainly of dissolved organic material initiates to form almost immediately (Shifeng, Nov 2012). Next microorganisms initiate to colonise the surface in a layer referred to as microfouling, including fungi, algae, bacteria, and diatoms. This layer starts forming within hours of immersion. Next, larvae of larger marine invertebrates such as bryozoans, mussels, barnacles, and polychaetes begin to attach to the microfouled surface in a layer referred to as macrofouling (Shifeng, Nov 2012) (Callow, 2002). This formation might be expected to start forming within two to three weeks of immersion (Railkin, 2004). The development of these biofouling layers is dependent on a combination of different environmental conditions like salinity, temperature, conductivity, pH, dissolved oxygen content, organic material content, hydrodynamic conditions, currents, light, depth, and distance from the shore (Delauney, 2009). In the following figure, a schematic of biofouling formation and build up, from the initial stage organic material to microfouling then macrofouling after, relative to several minutes, hours and weeks respectively, is presented.

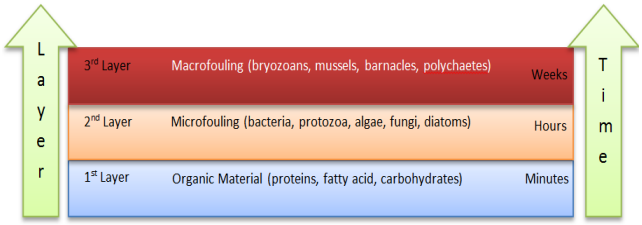


**Fig.1 A schematic plot of relative growth of biofouling with time and different layers.**

## 3 Modelling Approach and Results

### 3.1 Modelling approach and characteristics

Finite Element Analysis (FEA) methods have been carried out to model the forces exerted by ultrasonic plate waves in a ship hull, on the biochemical macromolecules and bacteria present in water, before they form a microfouling and macrofouling layers respectively. Target of this experimentation is to find the optimum mode and frequency for fouling prevention i.e. the mode and the frequency in which the cyclic particle motions will exert maximum forces on macromolecules and bacteria. Properly–designed FEA models have been designed and implemented to accomplish this purpose, whereas this analysis is expected to provide significant inputs into the design and application of the high power ultrasound transducer setup (see next Section 4).

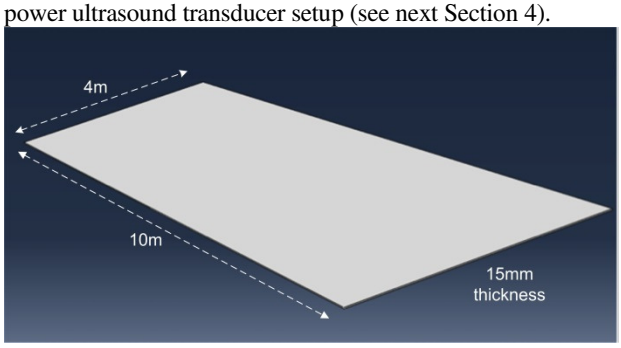


**Fig.2: Schematic representation of the 3D structure**

3D models were created based on the geometrical characteristics of the structure under investigation, as shown in Fig. 2. All FE modeling and analyses were carried out using the ABAQUS v6.12 general-purpose finite element program (Shifeng, Nov 2012). The characteristics of the finite element mesh of the 3D structure are given in the following. The plate structure is meshed with 8 elements through the thickness (test calculations have been run with 16 & 32 elements in thickness to ensure accuracy requirements are meet). To match the shape constraints the length and width of the elements had to be similar to the one in the direction of thickness.

The higher tensile 'AH36' grade 'A' alloy properties were used in our simulation. To perform the calculations required to simulate the transmission of an ultrasonic wave through

the hull structure the following material properties were utilized.

**Table 1 Material properties of the steel alloys used in our simulations**

| Property | Value | Unit in S.I |
|---|---|---|
| Young Modulus, E | $210*10^9$ | Pa |
| Poisson Ration, ν | 0.3 | [dimensionless] |
| Density, ρ | 7800 | $kg/m^3$ |

### 3.2 Dispersion curves

The selection of a suitable Lamb mode is fundamental to our work. The aim of long-range inspection is to investigate large areas rapidly. Hence, dispersion is a key factor and modes with low dispersion have to be chosen whereas the signal to noise ratio needs to be as high as possible to maximize the range of inspection. In the present case, S0 mode at frequencies lower than 100 kHz presents an almost non-dispersive behavior (Fig.3a). For a deeper insight on the investigation of the dispersive modes at low frequencies, Fig.3b gives a focused representation of the dispersion curves on a limited frequency range [0, 200kHz]. It is verified that S0 is the less dispersive mode, whereas A0 mode could be considered adequately non dispersive within a small frequency range. The results of this study were used for further analysis using Abaqus, where all the main wave modes (symmetric, anti-symmetric and shear) were further tested analytically within the aforementioned 'less dispersive' frequency range of [20kHz, 100kHz].

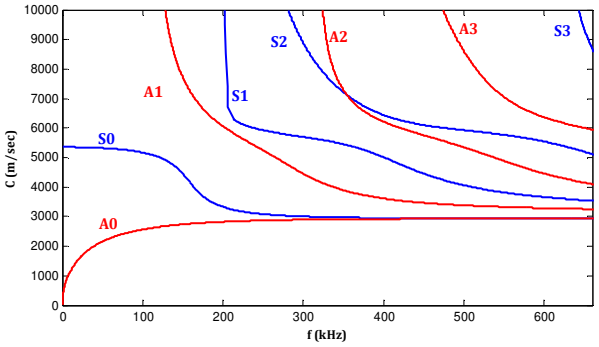


(a)

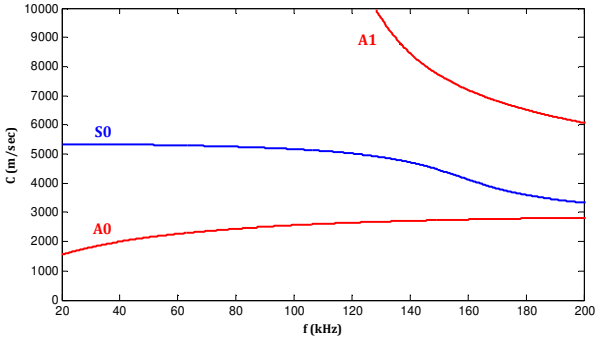


(b)

**Fig.3 Dispersion curve: (a) phase velocities (m/s) of various modes as a function of frequency (kHz) and (b) a low frequency representation of the phase velocities.**

### 3.3 Wave mode performance

Displacement and acceleration measures at a pre-defined location 1.5 m away from the transmitting point will be used as the main information criterion for comparisons along the three directions (x, y and z axis). Acceleration was employed as the final indicator as is directly correlated with the force development. Figure 4 shows an indicative frame-to-frame representation of the anti-symmetric wave propagation at the frequency of 25kHz whereas Fig.5 depicts the displacement signals received at the selected point utilizing symmetric, anti-symmetric and shear wave mode propagation.

Based on Fig. 5, the following findings are drawn:

- In symmetric wave propagation, the y-axis receives the

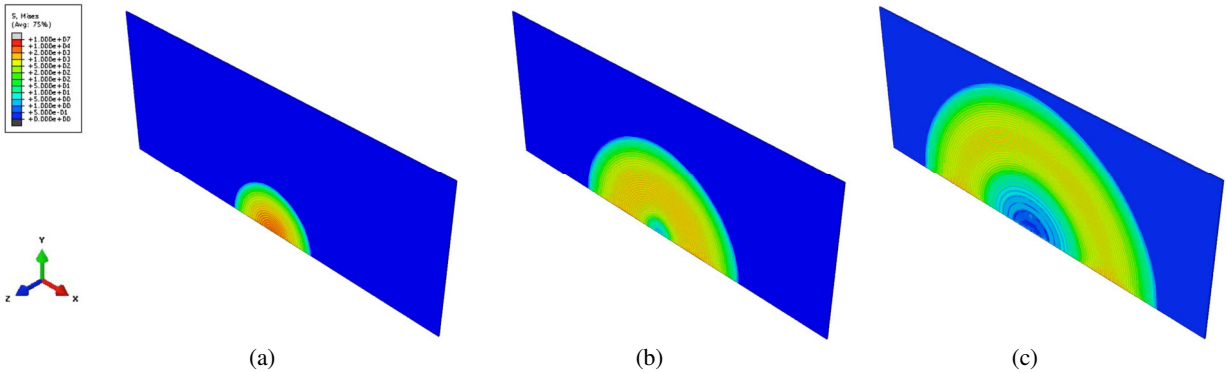

(a) (b) (c)

**Fig.4 Anti-symmetric wave propagation at the frequency of 25 kHz at various time instances: a) t=0.2ms, b) t=0.4ms and c) t=0.6ms.**

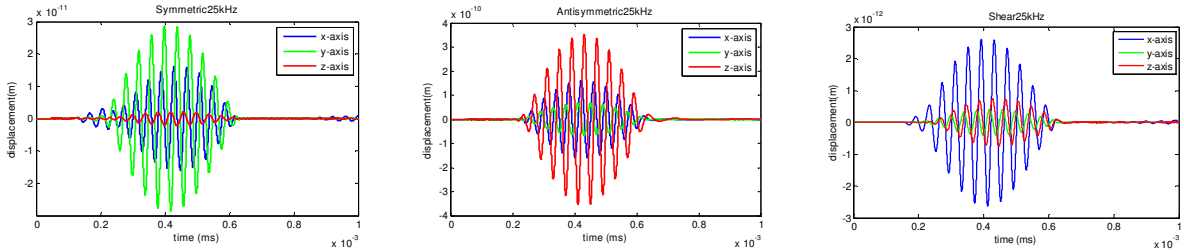


(a) (b) (c)

**Fig.5 Displacement signals received at the selected check point at 25kHz using (a) symmetric, (b) anti-symmetric and (c) shear wave modes.**

highest displacement values, whereas the x-axis receives moderate values (almost half compared with the corresponding ones from y-axis). The displacement values along the z-axis are significantly reduced in comparison with the other two directions.

- In the antisymmetric wave propagation, the z-axis receives the highest displacement values in comparison with the other two directions (x and y axes). This finding implies that this wave mode travels via flexural/ compressional motion maximizing the off-the-plate perpendicular movements (across the z-axis).
- Shear waves travel via a shearing motion with their maximum displacement values along the x-axis. The lowest absolute displacement and accelerations values among the three wave modes are observed (lower than $3*10^{-12}$).

To select the optimum wave mode for fouling prevention, a thorough comparison between symmetric and antisymmetric waves all over the frequency range will be performed in the following sections.

### 3.4 Selection of the optimum wave mode

To accomplish this task, a new measure was calculated that quantifies the global wave propagation along the three directions (x, y and z) providing a general informative indicator. The proposed acceleration magnitude ($\boldsymbol{acc_m}$) is defined as given in the following:

$$acc_m = \sqrt{(acc_x^2 + acc_y^2 + acc_z^2)} \qquad (1)$$

Where $acc_x$ , $acc_y$ and $acc_z$ denote the acceleration components received at x, y and z axis, respectively. This value quantifies the wave acceleration globally considering the information from the three directions (x-axis, y-axis and z-axis). Fig.6 depicts the acceleration magnitudes for anti-symmetric and symmetric waves as received in the selected check edge point.

Table 2 cites the maximum acceleration magnitudes achieved from symmetric and anti-symmetric waves in the

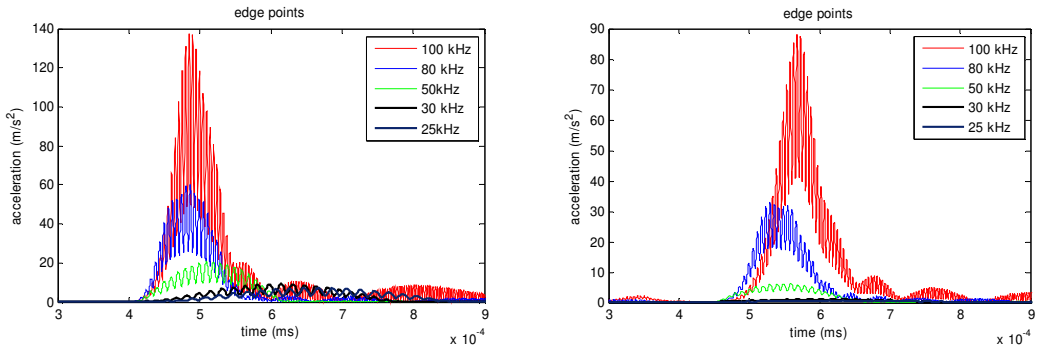


(a) (b)

**Fig.6 Acceleration magnitudes for antisymmetric (a) and symmetric (b) waves for frequency: 25kHz (dark blue), 30 kHz (black), 50 kHz (green), 80 kHz (blue) and 100 kHz (red), as received in the selected check edge point.**

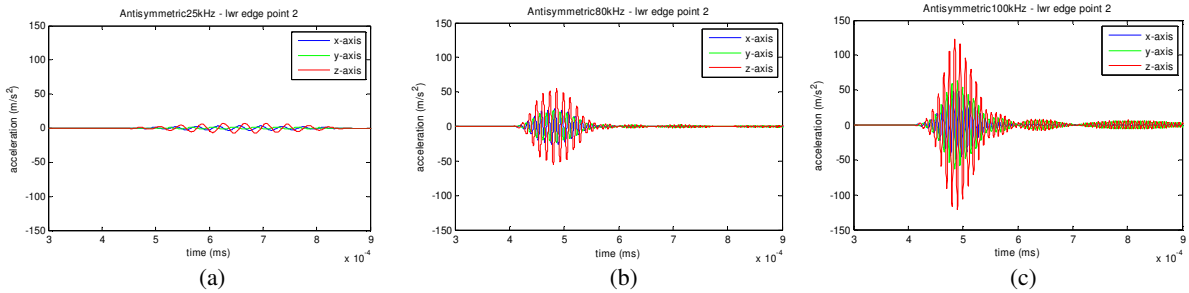


(a) (b) (c)

**Fig.7 Acceleration components in the axis: x (blue color), y (green color) and z (red color) received at different frequencies: a) 25kHz, b) 50 kHz and c) 100 kHz using anti-symmetric wave mode propagation.**

selected check point at each single frequency considered. The anti-symmetric waves prevail over the symmetric waves in all the frequencies considered indicating that anti-symmetric wave propagation is the optimum for fouling prevention since it maximizes the acceleration magnitudes and, therefore, the out-off-the-plate forces that can be applied on the attached on the surface bacteria.

**Table 2 Maximum acceleration ($ms^{-2}$) achieved at different frequencies**

| Wave mode / frequency | 25kHz | 30kHz | 50kHz | 80kHz | 100kHz |
|---|---|---|---|---|---|
| Symmetric | 0.7 | 1.2 | 6.3 | 32.8 | 88.2 |
| Antisymmetric | 7.3 | 9.3 | 20.8 | 59.9 | 137.4 |

### 3.5 Selection of the optimum frequency

The aforementioned results showed that anti-symmetric waves travelling at high frequencies (100kHz) generate higher acceleration magnitudes and, therefore, larger forces applied on the attached bacteria.

To accomplish a deeper investigation on the optimum frequency, a complementary analysis was performed where the x, y and z components of acceleration were separately assessed under various frequencies. It is shown in Fig.7, the highest frequency (100kHz) maximizes the z-component of acceleration that is linearly related with the perpendicular off-the-plate surface force that can be applied on the attached bacteria. A following clear pattern is observed: the higher the frequency, the larger the force off-the-plate applied on the bacteria. However, it is also presumed that the small forces received in low frequencies remain for large time periods. As frequency increases progressively higher forces can be generated, though their time durations decrease inversely proportionally. Consequently setting as the sole target the maximization of the force acting on the bacteria, the optimum frequency is the highest possible. However in more realistic considerations, a trade-off between maximum force and time duration could be preferred selecting slightly lower frequencies within a range of [20kHz, 100kHz]. In Section 4, frequencies within this non-dispersive range have been investigated experimentally in terms of their suitability to prevent the biofouling formation and buildup.

## 4 Experimental Investigation and Results

### 4.1 Vibrometry analysis of the fundamental modes propagating through a ship hull sample plate

The aim of these experiments is to analyse the influence of water in the opposite side of the transducers of the ship hull at two frequencies between 20kHz - 100kHz which are typically used for the inhibition of biofouling in ship hulls. The vibrometer used for measurements was a Polytec PSV400 3D Scanning Vibrometer (http://www.polytec.com).

#### 4.1.1 Vibrometer setup and procedure

Figure 8 shows the vibrometry setup which consists of the following components: 1), 2) and 3) are the vibrometer heads, 4) is the transducer holder with a high power transducer inside, 5) is the sample plate under analysis which simulates a part of a ship hull, 6) is the vessel that contains the water, and 7) is the water.
The sample plate under investigation is a S255 grade 'A' uncoated steel plate with mechanical properties (at 20°C) as follows; tensile stress: 370 MPa, yield stress: 245 MPa, specific elongation at fracture: 25%. The chemical composition of the same is as follow; C: max 0.22, Si: 0.15-0.3, Mn: max 0.65, Ni: max 0.3, S max 0.05, P: max 0.04, Cr: max 0.3, N: max 0.012, Cu: max 0.3 (S255 - Steel for structural constructions. Marochnik).

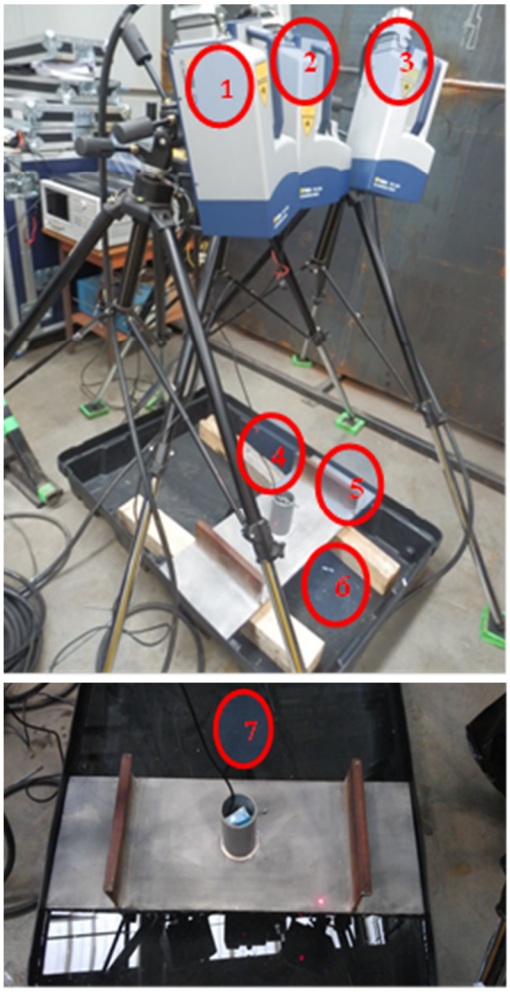


(a)

(b)

**Fig. 8 Vibrometer setup for the analysis of the influence of the water in the wave propagation in a 1.5cm thickness plate with stiffeners simulating a typical ship hull plate close to real conditions.**

First transducer with lower frequency is allocated in the transducer holder 4) and attached to the plate with a spring that wiled 20N constantly. Then with a signal generator the transducer is excited at its resonance frequency. The actual vibration at each point of the plate surface is collected for each pulse excited and recorded by the vibrometer. This

procedure is repeated with the second transducer of higher frequency but with the only in half of the plate. Afterwards the vessel is filled with water and the experiments are repeated with the two transducers.

### 4.1.2 Vibrometer results

Figure 9 and 10 show the RMS distribution of the wave propagation measured by the vibrometer. It can be seen that some nodes and antinodes are produced due to the creation of multiple reflexions from the features with different acoustic impedance such as edges and the stiffeners. On the antinodes the velocity and, therefore, the displacement is larger than in any other location and at the nodes the average displacement is lower.

The transducers in use are compressional transducer, therefore, it should be expected that some energy will be leakage to the water, although the water has very different acoustic impedance than the steel therefore, the water is expected to increase the attenuation of the wave propagation. It can be seen in Fig. 9 and 10 that the attenuation is larger when water is added.

At lower frequency, the distribution of energy is more even when the experiments are performed in dry conditions (Figure 9a). In the case of water (Figure 9b), the RMS of energy is much higher at the locations near to the transducers due to the amount of power transferred to the water of the other side of the plate.

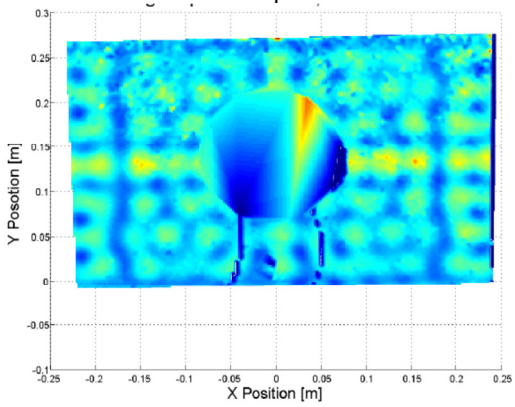


(a)

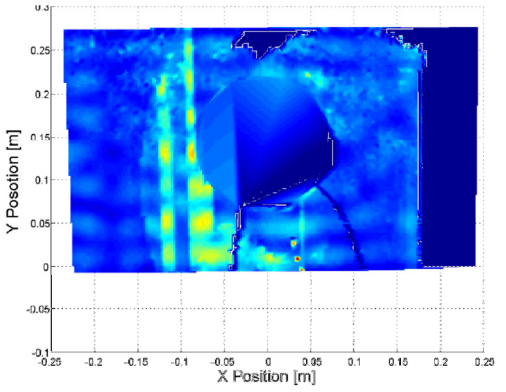


(b)

**Fig. 9 RMS displacement of a lower frequency acoustic wave**

On the other hand although the distribution is more even in the case of no water for the higher frequency the amount energy leakage to the water for this frequency is less important. In this second case it can be seen that due to the even distribution of energy the contribution of nodes and antinodes is less efficiency.

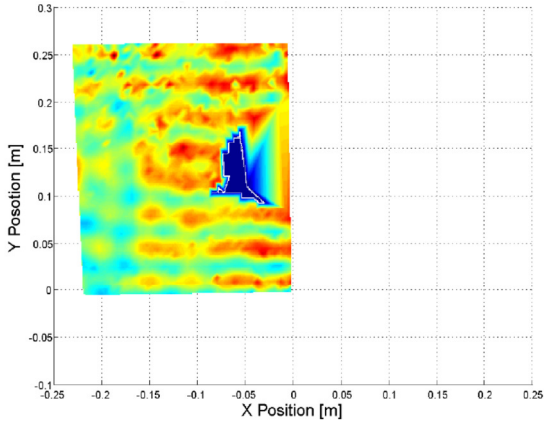


(a)

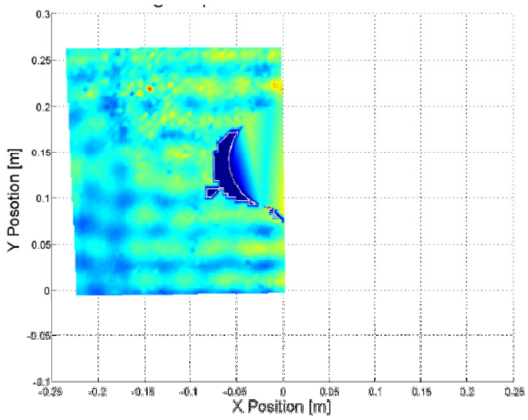


(b)

**Fig. 10 RMS displacement of a higher frequency acoustic wave**

## 4.2 Two transducers array optimization

In order to find the optimum array arrangement of transducers to create even & optimum energy distribution on steel plate, two experiments were carried out by BIC.

### 4.2.1.1 In-plate displacement detection experiment

In the first experiment, eight transducers were fixed on a surface of a 2x1m steel plate of 15mm thickness and grade ABS AH36. The mechanical properties of plate are as follows; min yield: 355 MPa, tensile: 490-620 MPa, longation: 21% The chemical composition of the same is as follows; C: 0.08, Si: 0.2, Mn: 0.68, P: 0.018, S: 0.009, V: 0.001, AL: 0.041, Cr: 0.032, Cu: 0.012, Mo:<0.003, Nb: <0.002, Ni: 0.011, Ti: 0.001. Two of the eight transducers were high power piezoelectric transducers used for generating vibrations (transmission) and an array of the rest six receiving transducers were used to measure those vibrations. The arrangement of the receiving transducers on

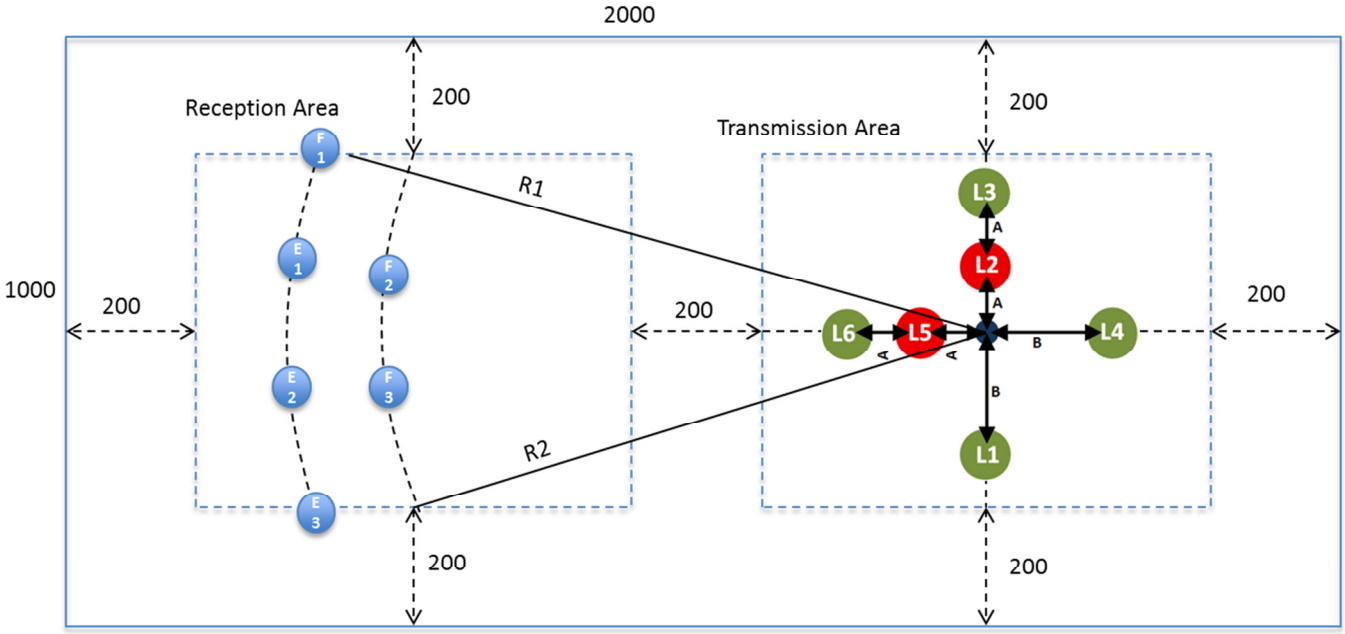


**Fig.11 In-plate Displacement Experiment Arrangement**

plate was fixed for a range of different arrangements of the two transmitting transducers. The general layout is shown in the figure 11.

E1, E2, E3, F1, F2 and F3 (E and F is the serial number identification) are the six transducers used to receive/measure vibrations at the reception area. As shown in the Figure 11, E1, E2, E3 and F1 are equally distributed at a radial distance of 'R1' from the center of transmission area. Transducers F2 and F3 are at a distance 'R2' from the centre of transmission area. Teletest M3 by Plant Integrity (Teletest Focus - Plant Integrity, 2014) was used to excite the transmitting transducers as well as to measure the wave produced in the receiving transducers. For each setup a frequency sweep of 20 to 100 kHz was applied. Amplitude of the vibrations measured was summed up to get the overall picture of the energy distribution at each location of receiving transducer for each setup. These summed up amplitudes are later compared with the highest sum of amplitude achieved throughout the experiment in terms of percentage. As mentioned earlier, the experiment was carried out with 6 different setups i.e. arrangements of transmitting transducers for which the locations of all six receiving transducers were fixed.

Various locations of transmitting transducers for each setup are shown within the transmission area in figure 11. Results from all setups are discussed later:

**Table 3: Locations of Transmitting Transducers**

| Setup | Number of Transducers | Locations |
|---|---|---|
| 1 | 1 | L1 |
| 2 | 2 | L1, L3 |
| 3 | 2 | L1, L2 |
| 4 | 1 | L4 |
| 5 | 2 | L4, L5 |
| 6 | 2 | L4, L6 |

#### 4.2.1.2 In-plate Displacement Detection Results

The amplitudes achieved at each location for the range of frequencies from 20 kHz to 100kHz are summed for all setups. These results are displayed below in tabular format showing the percentage of each summation of amplitudes compared with the highest summation of amplitude achieved during the experiment.

**Table 4: In-Plate Displacement Experiment Results**

| | E1 | E2 | E3 | F1 | F2 | F3 |
|---|---|---|---|---|---|---|
| Setup 1 | 21% | 50% | 68% | 56% | 8% | 78% |
| Setup 2 | 33% | 63% | 79% | 76% | 11% | 95% |
| Setup 3 | 29% | 53% | 77% | 69% | 11% | 100% |
| Setup 4 | 15% | 25% | 45% | 35% | 6% | 39% |
| Setup 5 | 16% | 25% | 41% | 33% | 6% | 42% |
| Setup 6 | 15% | 28% | 53% | 41% | 6% | 48% |

The figures below shows a comparison of the all six setups and locations in reception area gets the maximum energy. Amplitudes for all transducers for each setup are summed and compared with the max sum of amplitudes in terms of percentage in the Figure 12 below. Also, amplitudes for all setups for each location are summed and compared in Figure 13.

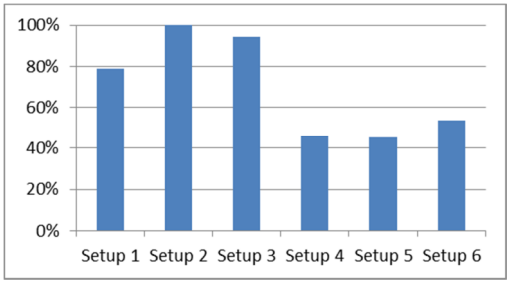


**Fig.12 In-Plate Displacement Detections Setups' Comparison**

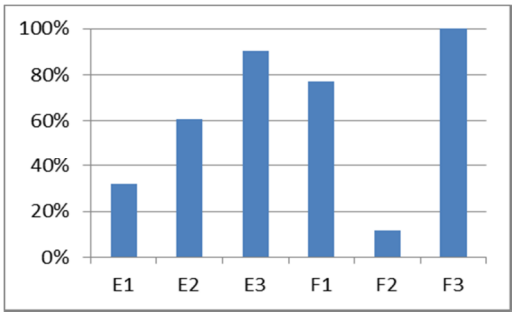


**Fig.13 In-Plate Displacement Detection Energy Distribution**

It can be observed that setups 1, 2 and 3 with one or two transducers located vertically dispel more energy compared to the horizontal arrangement of transducers. It can also be observed that E3, F1 and F3 receive more energy. This could be due to the reflections of waves from the edges of the plate causing constructive interference.

### 4.2.2.1 Out-plate displacement detection experiment methodology & setup

Experiment 2 was also conducted on the same steel plate. In experiment 2, two transducers both with the same resonance frequency in the range of 40 to 50kHz were used to transmit and 4 high power transducers (B1, B2, C1 and C2) (Where B and C are the channels of excitation) were used to receive. Locations of the receiving transducers were fixed throughout the experiment. In order to ensure highest magnitude of displacement on plate, constructive interferences are required at each point of the surface under analysis. The positions of the transmitting transducers were allocated with the aim to achieve wave reinforcement and hence the wavelengths were taken into account.. The wavelength was calculated from the dispersion curves calculated by the modelling Figure 3.

The same Teletest Mk 3 unit was used to generate a range of 10 kHz frequency sweep In this set of experiments two different distances between transducers were applied. First distance 'X' is calculated to enhance $A_0$ (Asymmetric waves). The second distance 'Y' is calculated to enhance $S_0$ (Symmetrical waves. Six different experiments were done with different transducers distances and angles. General Layout of all setups is displayed above in figure 14. The receiving transducers were located at random positions which were unchanged throughout the experiment. Setups 1, 3 and 5 were aimed to enhance $A_0$ and cancel partially the $S_0$. Therefore positioning two transmitting transducers horizontally, vertically and diagonally respectively with a distance of 'X' apart (equidistant from the center of transmission area) we can produce the type of interferences that we want. Setups 2, 4 and 6 used same arrangements with a different value for λ to enhance $S_0$ and cancel partially $A_0$ the two transducers 'Y' apart. 'X' and 'Y' here are optimum distances calculated taking respective wavelengths into account.

### 4.2.2.2 Out-plate displacement detection results

Displayed bellowed is a table with percentage of sum amplitudes for each transducers compared to maximum summation of amplitudes obtained for all transducers throughout the experiment. Below that (labelled as overall) the summation of amplitudes is compared to the highest maximum summation in terms of percent, Table 5.

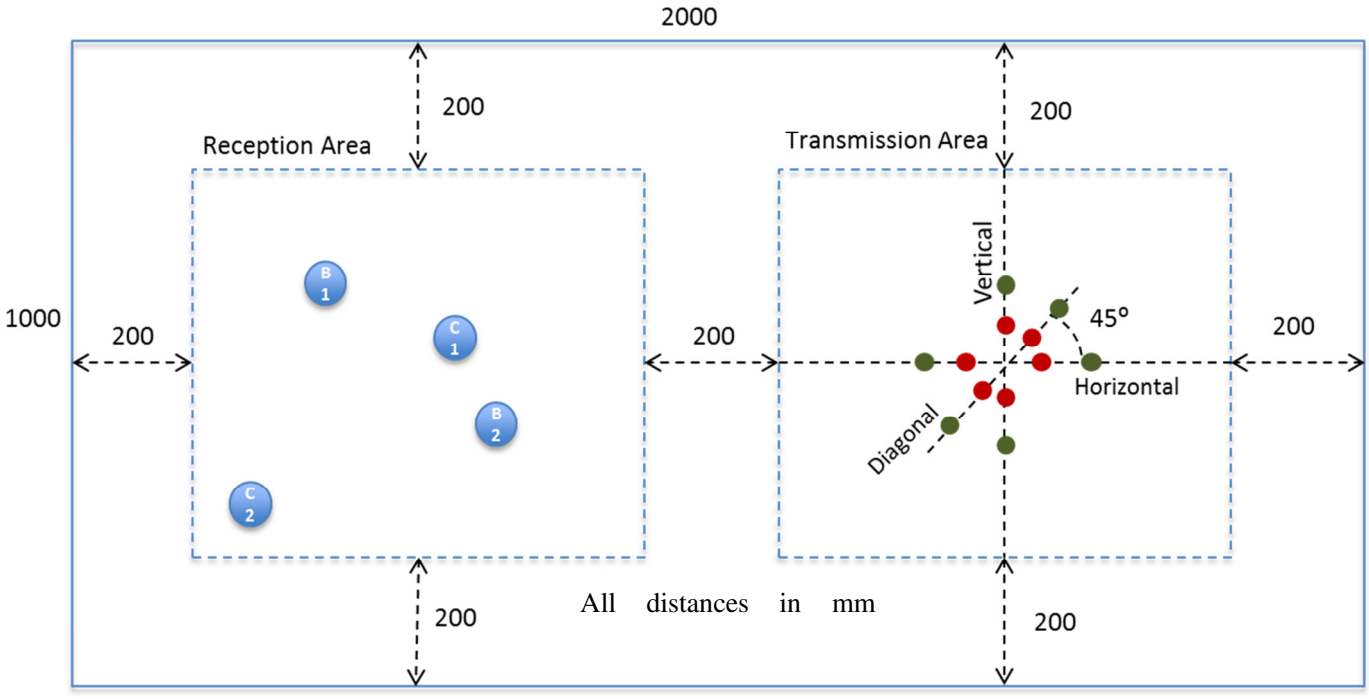


**Fig.14 Exp 2: Out-Plate Displacement Detection Experiment Setup**

**Table 5 Out-Plate Displacement Detection Results**

| | Setup 1 | Setup 3 | Setup5 | Setup 2 | Setup 4 | Setup 6 |
|---|---|---|---|---|---|---|
| B1 | 25% | 18% | 50% | 33% | 16% | 19% |
| B2 | 36% | 38% | 66% | 56% | 24% | 29% |
| C1 | 90% | 100% | 86% | 93% | 87% | 48% |
| C2 | 30% | 52% | 32% | 41% | 30% | 11% |
| Overall | 77% | 89% | 100% | 96% | 67% | 46% |
| Orientation | Horizontal | Vertical | Diagonal | Horizontal | Vertical | Diagonal |
| Transducer's Distance | | 'X' | | | 'Y' | |
| Wave Mode Enhancement | | $A_0$ | | | $S_0$ | |

Figure 15 shows the same comparison plotted in a bar chart. The same was done for each transducer location in the reception area and the results are plotted in Figure 16.

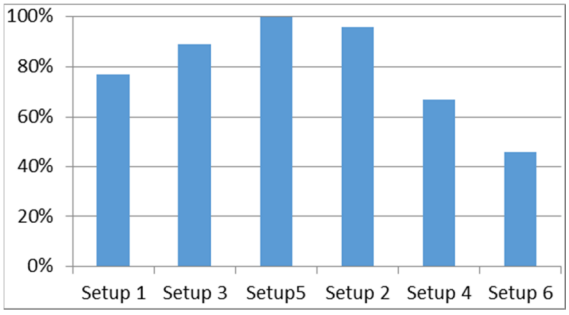


**Fig.15 Out-Plate Displacement Detection Experiment Setups Comparison**

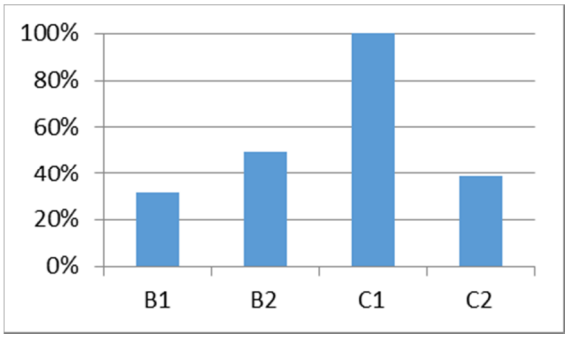


**Fig.16 Out-Plate Displacement Detection Experiment Energy Distribution**

It can be observed from the graphs plotted above that in general Setups 1, 3 and 5 that enhances $A_0$ mode of waves dispel more energy and is best for the purpose. While exciting $A_0$ mode, the vertical setup gives more energy compared to the horizontal setup however while exciting $S_0$ mode, the horizontal setup gives far more energy compared to the vertical setup.

Off all the various setups that the experiments were conducted with, Setup 5 of the Out-Plate Displacement Detection experiment where the two high power transmitting transducers were arrange diagonally at a distance 'X' apart aimed to enhance $A_0$ mode of waves seems to transfer maximum energy and more even energy distribution.

## 5 Conclusions and future works

In this paper, a preliminary study about the characterization of the ultrasonic wave propagation in the application of prevention of fouling in steel plate using an array of two compressional transducers, has been presented. Acoustic techniques for biofouling prevention have been proposed as a potential solution. According to the proposed modelling investigation, the antisymmetric wave propagation is the optimum for fouling prevention since it maximizes out-off-the-plate displacements could be applied on the attached microorganisms. A further study was done in an extensive experimental setup, where the investigation of a ultrasonic transducers array was performed. The results also conclude that the antisymmetric mode could be optimum for fouling prevention. On the other hand the wave reflection from the edges of the plate can modify the wave superimposition which in turn may changes the results of energy distribution.

Moreover, further investigations should focus on studying of the ultrasonic wave propagation in a larger representative plate and/or ship hull using an array with probably more than two compressional transducers.

## Acknowledgement

The research leading to these results has received funding from the European Union's Seventh Framework Programme managed by REA Research Executive Agency http://ec.europa.eu/research/rea([FP7/2007-2013]) for the project entitled "Prevention and detection of fouling on ship hulls" CLEANSHIP, under grant agreement no [312706], FP7-SME-2012-1 (http://cleanship-project.eu/). CLEANSHIP is collaboration between the following organisations: Brunel University, CERTH, Tecnalia, Enkon, Sofchem, WRS Marine, InnotecUK, and Lloyds's Register.

## References


Band, A. M. (n.d.). Transactions of the Oceanographic Commission USSR 13 (7).

Bott, T. (2000). Biofouling control with ultrasound. *Heat Transfer Engineering, 21*(3), 43-49.

Branscomb, E. S. (1984). An investigation of low frequency sound waves as a means of inhibiting barnacle settlement. *Journal of experimental marine biology and ecology, 79*(2), 149-154.

Callow, M. E. (2002). Marine biofouling: a sticky problem. *Biologist, 49*(1), 1-5.

Choi, C. a. (2013). The effect of vibration frequency and amplitude on biofouling deterrence. *Biofouling, 29*(2), 195-202.

David Blythe Foster, M. H. (1954, December 8). *Patent No. GB 719650 A*. United Kingdom.

Delauney, L. C. (2009). Biofouling protection for marine environmental sensors. *Ocean Science Discussions, 6*(4), 2993–3018.

Fischer, E. C. (1984). Technology for control of marine biofouling—a review. *Marine biodeterioration: an interdisciplinary study*, 261-299.

G Mazue, R. V.-Y. (2011). Large-scale ultrasonic cleaning system: Design of a multi-transducer device for boat cleaning (20kHz). *Ultrasonics Sonochemistry, 18*(4), 985-900.

Gavand, M. R. (2007). Effects of sonication and advanced chemical oxidants on the unicellular green alga dunaliella tertiolecta and cysts, larvae and adults of the brine shrimp artemia salina: A prospective treatment to eradicate invasive organisms from ballast water. *Marine pollution bulletin, 54*(11), 1777-1788.

Gittens, J. E. (2013). Current and emerging environmentally-friendly systems for fouling control in the marine environment. *Biotechnology advances, 31*(8), 1738-1753.

Kitamura, H. a. (1995). Inhibitory effect of ultrasonic waves on the larval settlement of the barnacle, Balanus amphitrite in the laboratory. *付着生物研究, 12*(1), 9-13.

Latour, M. a. (1981). Application of PVF2 transducers as piezoelectric vibrators for marine fouling prevention. *Ferroelectrics, 32*(1), 33-37.

Morley, C. O. (1954, January 27). *Patent No. GB 703158 A*. United Kingdom.

P. S. Sheherbakov, F. Y. (1974). *TRANSACTIONS. TECHNICAL OPERATIONS OF THE MARITIME FLEET. THERMOCHEMICAL STUDIES. CONTROL OF CORROSION AND FOULING. CENTRAL SCIENTIFIC RESEARCH INSTITUTE OF THE MARITIME FLEET.* Naval Intelligence Support Center.

Piper, S. D. (1977, Nov 15). *Patent No. US 04058075*. United States of America.

Railkin, A. I. (2004). *Marine biofouling: colonization processes and defenses* (Vol. 20). Taylor & Francis.

*S255 - Steel for structural constructions. Marochnik*. (n.d.). Retrieved May 2014, from http://www.splav-kharkov.com/en/e_mat_start.php?name_id=884

Shifeng, G. (Nov 2012). *A Study of Ultrasonic Effects on the Marine Biofouling Organism of Barnacle, Amphibalanus Amphitrite.* Thesis, MECHANICAL ENGINEERING.

*Sofchem, distributeur et installateur de la technologie anti algues Fluid Impact*. (n.d.). Retrieved January 2014, from http://www.sofchem.fr/antialgues_fluid_impact.htm

*Teletest Focus - Plant Integrity*. (2014, May 5). Retrieved from http://www.plantintegrity.com/teletest/

Yebra, D. M.-J. (2004). Antifouling technology—past, present and future steps towards efficient and environmentally friendly antifouling coatings. *Progress in organic coatings, 50*(2), 75-104.